# Determination of the parameters of a Skyrme type effective interaction using the simulated annealing approach

B. K. Agrawal, S. Shlomo, and V. Kim Au
*Cyclotron Institute, Texas A&M University, College Station, Texas 77843, USA*
(Received 7 September 2004; revised manuscript received 12 May 2005; published 21 July 2005)

We implement for the first time the simulated annealing method to the problem of searching for the global minimum in the hypersurface of the $\chi^2$ function, which depends on the values of the parameters of a Skyrme-type effective nucleon-nucleon interaction. We undertake a realistic case of fitting the values of the Skyrme parameters to an extensive set of experimental data on the ground-state properties of many nuclei, ranging from normal to exotic ones. The set of experimental data used in our fitting procedure includes the radii for the valence $1d_{5/2}$ and $1f_{7/2}$ neutron orbits in the $^{17}$O and $^{41}$Ca nuclei, respectively, and the breathing-mode energies for several nuclei, in addition to the typically used data on binding energy, charge radii, and spin-orbit splitting. We also include in the fit the critical density $\rho_{cr}$ and further constrain the values of the Skyrme parameters by requiring that (i) the quantity $P = 3\rho(dS/d\rho)$, directly related to the slope of the symmetry energy $S$, must be positive for densities up to $3\rho_0$; (ii) the enhancement factor $\kappa$, associated with the isovector giant dipole resonance, should lie in the range of 0.1–0.5; and (iii) the Landau parameter $G_0'$ is positive at $\rho = \rho_0$. We provide simple but consistent schemes to account for the center-of-mass corrections to the binding energy and charge radii.

DOI: 10.1103/PhysRevC.72.014310 PACS number(s): 21.10.Dr, 21.10.Pc, 21.30.Fe, 21.60.Ka

## I. INTRODUCTION

Since the pioneering work of Brink and Vautherin [1], continuous efforts have been made to readjust the parameters of the Skyrme-type effective nucleon-nucleon interaction to better reproduce experimental data. Most of the parameters of the Skyrme interactions available in the literature were obtained by the fitting of the Hartree-Fock (HF) results to experimental data on bulk properties of a few stable closed-shell nuclei. Only recently, several families of the Skyrme parameters, e.g., SkI1-6, SLy1-10, SKX, and SkO [2–7], were obtained by the fitting of HF results to the experimental data on the bulk properties of nuclei ranging from the $\beta$-stable nuclei to those near the proton and/or neutron drip lines. In the SKX interaction, to yield appropriately the values for the binding-energy differences between mirror nuclei, also referred to as the Coulomb displacement energy (CDE), the contribution of the Coulomb exchange term in the HF equations is ignored and the direct Coulomb term is evaluated by replacement of the point-proton distribution by its charge distribution. However, it has been further shown in Ref. [8] that the SKX interaction is not suitable for studying the properties of neutron stars because, for the SKX interaction, the quantity

$$P = 3\rho\frac{dS}{d\rho}, \tag{1}$$

which is directly related to the slope of the symmetry-energy coefficient $S$, becomes negative for nuclear matter densities $\rho$ well below $3\rho_0$ ($\rho_0 = 0.16$ fm$^{-3}$ is the saturation density). On the other hand, the SkI1-6, SLy1-10, and SkO Skyrme interactions are found to be suitable for the study of neutron stars [8]. However, these families of Skyrme interactions significantly underestimate the values of the CDE for mirror nuclei because the Coulomb exchange term was included. Thus it is desirable to have a unified interaction that includes the merits of several families of the Skyrme interactions, as already mentioned. One can further enhance the applicability of the Skyrme-type effective $NN$ interaction by imposing certain constraints, as subsequently discussed.

The aim of this work is twofold. We implement, for the first time, the simulated annealing method (SAM) [9,10] to fit the values of the Skyrme parameters and develop a more realistic Skyrme-type effective interaction. The SAM is an elegant technique for optimization problems of large scale, in particular, where a desired global extremum is hidden among many local extrema. This method has been found to be an extremely useful tool for a wide variety of minimization problems of large nonlinear systems in many different areas of science (e.g., see Refs. [11–13]). Very recently [14,15], the SAM was used to generate some initial trial parameter sets for the point-coupling variant of the relativistic mean-field model. In the present context, we use the SAM to determine the values of the Skyrme parameters by searching for the global minimum in the hypersurface of the $\chi^2$ function, given as

$$\chi^2 = \frac{1}{N_d - N_p}\sum_{i=1}^{N_d}\left(\frac{M_i^{\rm exp} - M_i^{\rm th}}{\sigma_i}\right)^2 \tag{2}$$

where $N_d$ and $N_p$ are the number of experimental data points and the number of fitted parameters, respectively, $\sigma_i$ is the theoretical error, and $M_i^{\rm exp}$ and $M_i^{\rm th}$ are the experimental and the corresponding theoretical values, respectively, for a given observable. The values of $\chi^2$ depend on the Skyrme parameters, because, the $M_i^{\rm th}$ in Eq. (2) is calculated with the HF approach with a Skyrme-type effective nucleon-nucleon interaction.

Toward the purpose of obtaining a more realistic parametrization of the Skyrme interaction, we apply the SAM to fit the HF results to an extensive set of experimental data for the binding energy, charge radii, spin-orbit splitting, and root-mean-square (rms) radii of valence neutron orbits. Our data set used in the fit consists of 14 spherical nuclei,

 

namely, $^{16}$O, $^{24}$O, $^{34}$Si, $^{40}$Ca, $^{48}$Ca, $^{48}$Ni, $^{56}$Ni, $^{68}$Ni, $^{78}$Ni, $^{88}$Sr, $^{90}$Zr, $^{100}$Sn, $^{132}$Sn, and $^{208}$Pb. We also include in our fit the experimental data for the breathing-mode energies for the $^{90}$Zr, $^{116}$Sn, $^{144}$Sm, and $^{208}$Pb nuclei. In addition, we include in the fit the critical density $\rho_{\rm cr}$, which is determined from the stability conditions for the Landau parameters [16,17]. We further constrain the values of the Skyrme parameters by requiring that (i) the quantity $P$ must be positive for densities up to $3\rho_0$, a condition imposed by neutron star models [8]; (ii) the enhancement factor $\kappa$, associated with the Thomas-Reiche-Kuhn (TRK) sum rule for the isovector giant dipole resonance, lies in the range of 0.1–0.5 [3,18–20]; and (iii) the Landau parameter $G_0'$, crucial for the spin properties of finite nuclei and nuclear matter, should be positive at $\rho = \rho_0$ [20,21]. We also provide simple but consistent schemes to account appropriately for the CDE and the center-of-mass (c.m.) corrections to the binding energy and charge radii. To check the reliability of the proposed Skyrme interactions for the study of high-density matter, we examine in detail the behavior of the symmetry energy and the nature of the equation of state (EOS) for pure neutron matter at densities relevant for the neutron star models.

We have organized our paper as follows. In Sec. II we briefly outline the form of the Skyrme nucleon-nucleon ($NN$) effective interaction and the corresponding energy-density functional adopted in the present work. In this section, we also provide feasible strategies for the calculations of CDE and the c.m. corrections to the total binding energy and charge radii. In Sec. III we provide the relations between the Skyrme parameters and the various nuclear matter properties, which we have used to implement the SAM algorithm, as described in Sec. IV. The set of the experimental data along with the theoretical errors and the constraints used in the fit to determine the values of the Skyrme parameters are given in Sec. V. In Sec. VI we present our results for the two different fits carried out in this work. Finally, in Sec. VII we summarize our main results and discuss the scope for further improvement of the present work.

## II. SKYRME ENERGY-DENSITY FUNCTIONAL

In this work we adopt the following form for the Skyrme-type effective $NN$ interaction [1,3]:

$$\begin{aligned} V_{12} &= t_0\left(1+x_0P_{12}^{\sigma}\right)\delta(\mathbf{r}_1-\mathbf{r}_2) \\ &+\frac{1}{2}t_1\left(1+x_1P_{12}^{\sigma}\right)\times\left[\overleftarrow{k}_{12}^{2}\delta(\mathbf{r}_1-\mathbf{r}_2)+\delta(\mathbf{r}_1-\mathbf{r}_2)\overrightarrow{k}_{12}^{2}\right] \\ &+t_2\left(1+x_2P_{12}^{\sigma}\right)\overleftarrow{k}_{12}\delta(\mathbf{r}_1-\mathbf{r}_2)\overrightarrow{k}_{12} \\ &+\frac{1}{6}t_3\left(1+x_3P_{12}^{\sigma}\right)\rho^{\alpha}\left(\frac{\mathbf{r}_1+\mathbf{r}_2}{2}\right)\delta(\mathbf{r}_1-\mathbf{r}_2) \\ &+iW_0\overleftarrow{k}_{12}\delta(\mathbf{r}_1-\mathbf{r}_2)(\overrightarrow{\sigma_1}+\overrightarrow{\sigma_2})\times\overrightarrow{k}_{12}, \end{aligned} \tag{3}$$

where $t_i$, $x_i$, $\alpha$, and $W_0$ are the parameters of the interaction and $P_{12}^{\sigma}$ is the spin-exchange operator, $\overrightarrow{\sigma_i}$ is the Pauli spin operator, $\overrightarrow{k_{12}}=-i(\overrightarrow{\nabla_1}-\overrightarrow{\nabla_2})/2$, and $\overleftarrow{k_{12}}=-i(\overleftarrow{\nabla_1}-\overleftarrow{\nabla_2})/2$. Here, the right and left arrows indicate that the momentum operators act on the right and on the left, respectively. The corresponding mean field $V_{\rm HF}$ and the total energy $E$ of the system are given by

$$V_{\rm HF}=\frac{\delta\mathcal{H}}{\delta\rho}, \qquad E=\int\mathcal{H}(r)d^3r, \tag{4}$$

where the Skyrme energy-density functional $\mathcal{H}(r)$, obtained with Eq. (3), is given by [1,3]

$$\mathcal{H}=\mathcal{K}+\mathcal{H}_0+\mathcal{H}_3+\mathcal{H}_{\rm eff}+\mathcal{H}_{\rm fin}+\mathcal{H}_{\rm so}+\mathcal{H}_{\rm sg}+\mathcal{H}_{\rm Coul}, \tag{5}$$

where, $\mathcal{K}=(\hbar^2/2m)\tau$ is the kinetic-energy term, $\mathcal{H}_0$ is the zero-range term, $\mathcal{H}_3$ the density-dependent term, $\mathcal{H}_{\rm eff}$ is an effective-mass term, $\mathcal{H}_{\rm fin}$ is a finite-range term, $\mathcal{H}_{\rm so}$ is a spin-orbit term, $\mathcal{H}_{\rm sg}$ is a term that is due to tensor coupling with spin and gradient, and $\mathcal{H}_{\rm Coul}$ is the contribution to the energy density that is due to the Coulomb interaction. For the Skyrme interaction of Eq. (3), we have

$$\mathcal{H}_0=\tfrac{1}{4}t_0\left[(2+x_0)\rho^2-(2x_0+1)\left(\rho_p^2+\rho_n^2\right)\right], \tag{6}$$

$$\mathcal{H}_3=\tfrac{1}{24}t_3\rho^{\alpha}\left[(2+x_3)\rho^2-(2x_3+1)\left(\rho_p^2+\rho_n^2\right)\right], \tag{7}$$

$$\begin{aligned}\mathcal{H}_{\rm eff} &= \tfrac{1}{8}[t_1(2+x_1)+t_2(2+x_2)]\tau\rho+\tfrac{1}{8}[t_2(2x_2+1) \\ &-t_1(2x_1+1)](\tau_p\rho_p+\tau_n\rho_n),\end{aligned} \tag{8}$$

$$\begin{aligned}\mathcal{H}_{\rm fin} &= \tfrac{1}{32}[3t_1(2+x_1)-t_2(2+x_2)](\nabla\rho)^2 \\ &-\tfrac{1}{32}[3t_1(2x_1+1)+t_2(2x_2+1)] \\ &\times[(\nabla\rho_p)^2+(\nabla\rho_n)^2],\end{aligned} \tag{9}$$

$$\mathcal{H}_{\rm so}=\frac{W_0}{2}[\mathbf{J}\cdot\nabla\rho+x_w(\mathbf{J_p}\cdot\nabla\rho_p+\mathbf{J_n}\cdot\nabla\rho_n)], \tag{10}$$

$$\mathcal{H}_{\rm sg}=-\tfrac{1}{16}(t_1x_1+t_2x_2)\mathbf{J}^2+\tfrac{1}{16}(t_1-t_2)\left[\mathbf{J_p}^2+\mathbf{J_n}^2\right]. \tag{11}$$

Here, $\rho=\rho_p+\rho_n$, $\tau=\tau_p+\tau_n$, and $\mathbf{J}=\mathbf{J_p}+\mathbf{J_n}$ are the particle number density, kinetic-energy density, and spin density, with $p$ and $n$ denoting the protons and neutrons, respectively. We have used the value of $\hbar^2/2m=20.734$ MeV fm$^2$ in our calculations. We would like to emphasize that we have included the contributions from the spin-density term as given by Eq. (11), which is ignored in many Skyrme HF calculations. Although the contributions from Eq. (11) to the binding energy and charge radii are not very significant, they are very crucial for the calculation of the Landau parameter $G_0'$ [22].

### A. Coulomb energy

The contribution to the energy density [Eq. (5)] from the Coulomb interaction can be written as a sum of a direct term and an exchange term:

$$\mathcal{H}_{\rm Coul}(r)=\mathcal{H}_{\rm Coul}^{\rm dir}(r)+\mathcal{H}_{\rm Coul}^{\rm ex}(r). \tag{12}$$

For the direct term it is common to adopt the expression

$$\mathcal{H}_{\rm Coul}^{\rm dir}(r)=\frac{1}{2}e^2\rho_p(r)\int\frac{\rho_p(r')d^3r'}{\mid\mathbf{r}-\mathbf{r}'\mid}, \tag{13}$$

and for the corresponding exchange term to use the Slater approximation [23]:

$$\mathcal{H}^{\rm ex}_{\rm Coul}(r) = -\frac{3}{4}e^2\rho_p(r)\left[\frac{3\rho_p(r)}{\pi}\right]^{1/3}. \qquad (14)$$

It is very important to emphasize that the definitions of Eqs. (13) and (14) are not for the bona fide direct and exchange terms, as each of them includes the contributions of the self-interaction, which appear in opposite signs and cancel out in Eq. (12). Note, in particular, that the direct term of Eq. (13) is proportional to $Z^2$ and not to $Z(Z-1)$, as it should be for a direct term; see a detailed discussion in Ref. [24]. We point out that for the CDE of mirror nuclei the magnitude of the self-interaction term is CDE/(2$Z$), i.e., one has a spurious increase in the calculated CDE of about 6.3% and 2.5% for the $A = 17$ and 41 systems of mirror nuclei, respectively.

We recall that, within the mean-field approximation, adjusted to reproduce the experimental values of the charge rms radii, the calculated CDE of analog states [obtained with Eq. (12)] are smaller than the corresponding experimental values by about 7%. It was first shown in Ref. [25] that this discrepancy, also known as the Nolen-Schiffer anomaly [26], can be explained when the contributions that are due to long-range correlations (LRCs) and to the charge symmetry breaking (CSB) in the *NN* interaction are taken into account; see also Ref. [27]. We add that for the mirror nuclei with $A = 17$ and $A = 41$, the LRC and the CSB each accounts for about half of the discrepancy between theory and experiment. Also, the magnitude of the bona fide exchange Coulomb term is about the same as that due to LRCs, but with opposite sign. Therefore, neglecting the bona fide Coulomb exchange term does not resolved the discrepancy between theory and experiment, but can account for the contribution of LRCs. We add that, in Ref. [28], it was shown that by ignoring the Coulomb exchange term in the form of Eq. (14) in Eq. (12), i.e., by including only the Coulomb direct term in the form of Eq. (13) (as is the case for the SKX interaction), one reproduces the experimental values of the CDE. It should be clear that this is due to the fact that by adopting the form of Eq. (13) for the Coulomb direct term one not only neglects the bona fide Coulomb exchange term, but also adds the spurious contribution of the self-interaction term. The unphysical neglect of the bona fide Coulomb exchange term together with the spurious contribution of the self-interaction term results in a contribution to CDE that is similar in magnitude to that obtained from the LRC + CSB terms. For simplicity, we adopt in this work the form of Eq. (13) for the Coulomb direct term.

### B. Center-of-mass corrections to the binding energy and charge radii

The HF approach applied to finite nuclei violates the translational invariance, introducing a spurious c.m. motion. Thus, one must extract the contributions of the c.m. motion to the binding energy $B$, radii, and other observables. An accurate way to restore the translational invariance is to use the projection method. However, it is numerically very expensive. Therefore, it is desirable to develop simple schemes for the c.m. corrections to various observables. Normally, one makes the c.m. corrections only to the binding energy and not to the radii. However, the c.m. corrections to the rms radii for light nuclei may be as large as 2% [24]. In the present work we consider the c.m. corrections to the binding energy as well as charge rms radii used to fit the Skyrme parameters.

To account for the c.m. correction to the total binding energy, one must subtract from it the so-called c.m. energy, given as

$$E_{\rm c.m.} = \frac{1}{2mA}\langle\hat{\mathbf{P}}^2\rangle, \qquad (15)$$

where $\hat{\mathbf{P}} = -i\hbar\sum_{i=1}^{A}\nabla_i$ is the total linear momentum operator. Traditionally, one simplifies the computation of Eq. (15) by taking into account only the one-body parts of it, which can be easily achieved by replacing $\frac{1}{m} \to \frac{1}{m}[1-\frac{1}{A}]$ in the kinetic-energy term. In this case, the effects of neglecting the two-body part of Eq. (15) are compensated for by renormalization of the force parameters. This may induce in the forces an incorrect trend with respect to $A$ that becomes visible in the nuclear matter properties. In fact, it is found in Ref. [29] that an oversimplified treatment of $E_{\rm c.m.}$ obtained by renormalization of the nucleon mass appearing in the kinetic-energy term leads to a larger value of the surface-energy coefficient than those obtained with the full c.m. correction. This gives rise to differences in the deformation energy that becomes quite pronounced for the superdeformed states. Very recently [17], we also find that a large value of the surface-energy coefficient yields a smaller value for the critical density. Thus an appropriate and still simple scheme to evaluate Eq. (15) is highly desirable. We note, however, that the SLy6, SLy7, and SLy10 interactions [4] have been obtained by evaluation of Eq. (15) [i.e., including the one- and two-body c.m. terms of Eq. (15)]. In the harmonic-oscillator (HO) approximation, $E_{\rm c.m.}$ of Eq. (15) is given by

$$E^{\rm HO}_{\rm c.m.} = \tfrac{3}{4}\hbar\omega. \qquad (16)$$

A value of $\hbar\omega = 41A^{-1/3}$ MeV is used in many relativistic mean-field calculations [30,31]. An improved version for the c.m. correction can be obtained by modification of the oscillator frequency as $\hbar\omega = 45A^{-1/3} - 25A^{-2/3}$ MeV, which has been used in Ref. [5] to obtain the SKX interaction. Here, we employ a simple but more consistent scheme to evaluate the $E_{\rm c.m.}$ by using the HO approximation. We determine the oscillator frequency $\hbar\omega$ appearing in Eq. (16) by using the mean-square mass radii $\langle r^2\rangle$ calculated in the HF approach as

$$\hbar\omega = \frac{\hbar^2}{mA\langle r^2\rangle}\sum_i\left[\mathcal{N}_i + \frac{3}{2}\right], \qquad (17)$$

where the sum runs over all the occupied single-particle states for the protons and neutrons and $\mathcal{N}_i$ is the oscillator quantum number. We emphasize that this scheme is quite reliable even for the nuclei away from the $\beta$-stable line, where the values of the rms radii deviate from the $A^{1/3}$ law. We have calculated the total binding energy for the SLy7 interaction by using our simple scheme for the c.m. correction, Eq. (17), and compare them with those given in Ref. [4], obtained by

using one- and two-body parts of the Eq. (15). For example, we find that for the $^{16}$O, $^{40}$Ca, $^{132}$Sn, and $^{208}$Pb nuclei the total binding energy $B = 128.65$ (128.55), 344.98 (344.90), 1102.38 (1102.77), and 1636.29 (1636.76) MeV, respectively; the values in parentheses are taken from Ref. [4]. This clearly indicates that the c.m. correction to the binding energy can be reliably estimated with Eq. (17). We would also like to remark, however, that the $E_{\rm c.m.}$ calculated with the oscillator frequency as $\hbar\omega = 45A^{-1/3} - 25A^{-2/3}$ MeV in Eq. (16) overestimates the value of binding energy in light nuclei (e.g., $^{16}$O and $^{40}$Ca) by about 1–2 MeV, which is quite significant.

The mean-square radius for the point-proton distribution corrected for the c.m. motion is obtained as [24]

$$\langle r_p^2\rangle = \langle r_p^2\rangle_{\rm HF} - \frac{3}{2\nu A}, \tag{18}$$

where $\nu = m\omega/\hbar$ is the size parameter. Therefore the corresponding mean-square charge radius to be fitted to the experimental data is obtained as

$$\langle r_{\rm ch}^2\rangle = \langle r_p^2\rangle_{\rm HF} - \frac{3}{2\nu A} + \langle r^2\rangle_p + \frac{N}{Z}\langle r^2\rangle_n + \frac{1}{Z}\left(\frac{\hbar}{mc}\right)\sum_{nlj\tau}(2j+1)\mu_\tau\langle\overrightarrow{\sigma}\cdot\overrightarrow{l}\rangle_{lj}, \tag{19}$$

where, $\langle r^2\rangle_p$ and $\langle r^2\rangle_n$ are the mean-squared radii of the proton and neutron charge distributions, respectively. The last term in Eq. (19) is due to the spin-orbit effect [32]. We use $\langle r^2\rangle_n = -0.12$ fm$^2$ and the recent [33] value of $\langle r^2\rangle_p = 0.801$ fm$^2$.

### C. Determination of the critical density

We use the stability conditions of the Landau parameters for the symmetric nuclear matter and pure neutron matter to calculate the critical density $\rho_{\rm cr}$ for the Skyrme-type effective *NN* interactions. The stability conditions are given as [34]

$$\mathcal{A}_l > -(2l+1), \tag{20}$$

where $\mathcal{A}_l$ are the Landau parameters $F_l$, $F_l'$, $G_l$, and $G_l'$ for a given multipolarity $l$. Skyrme interactions contain only monopolar and dipolar contributions to the particle-hole interaction so that all Landau parameters are zero for $l > 1$. Thus there are 12 different Landau parameters, i.e., $F_l$, $F_l'$, $G_l$ and $G_l'$ ($l = 0, 1$) for the symmetric nuclear matter and $F_l^{(n)}$, $G_l^{(n)}$ ($l = 0, 1$) for the pure neutron matter. Each of these parameters must satisfy the inequality condition given by inequality (20). Explicit expressions for the Landau parameters in terms of the Skyrme parameters can be found in Refs. [16,35]. The critical density is nothing but the maximum density beyond which at least one of the Landau parameters does not satisfy inequality (20). Following Ref. [16], one can obtain the values of the Landau parameters at any density for a given set of the Skyrme parameters. Thus, for a given set of Skyrme parameters, one can easily obtain the value of $\rho_{\rm cr}$. As mentioned in Sec. I, we include $\rho_{\rm cr}$ in the fit.

### D. Breathing-mode energy

We also include in our fit the experimental data on the breathing-mode energy for several nuclei. We consider the fully self-consistent values for the breathing-mode constrained energy, defined as

$$E_0 = \sqrt{\frac{m_1}{m_{-1}}}, \tag{21}$$

where $m_k$ are the energy moments,

$$m_k = \int_0^\infty \omega^k S(\omega)d\omega, \tag{22}$$

of the strength function

$$S(\omega) = \sum_n |\langle n|F|0\rangle|^2\delta(\omega-\omega_n), \tag{23}$$

for the monopole operator $F(r) = \sum_{i=1}^A f(r_i)$, with $f(r) = r^2$. The moments $m_k$ for $k = -1$ and 1 appearing in Eq. (21) can be obtained with the constrained HF (CHF) and the double-commutator sum rule, respectively [36–38]. The moment $m_1$ can be expressed in terms of the ground-state density $\rho$ as

$$m_1 = 2\frac{\hbar^2}{m}\langle r^2\rangle, \tag{24}$$

where

$$\langle r^2\rangle = \int r^2\rho(r)d\mathbf{r}. \tag{25}$$

As described in detail in Refs. [36–38], $m_{-1}$ can be evaluated by means of the CHF approach and is given as

$$m_{-1} = \frac{1}{2}\frac{d}{d\lambda}\langle r_\lambda^2\rangle\Big|_{\lambda=0} \tag{26}$$

where $\langle r_\lambda^2\rangle = \langle\Phi_\lambda|r^2|\Phi_\lambda\rangle$, where $\Phi_\lambda$ is the HF solution to the CHF Hamiltonian $H - \lambda f$.

## III. SKYRME PARAMETERS AND NUCLEAR MATTER PROPERTIES

In this section we discuss the relationship between the Skyrme parameters and the various quantities describing the nuclear matter. In the next section we use these relations to implement the SAM algorithm. The Skyrme parameters $t_i$, $x_i$, and $\alpha$ for a fixed value of $W_0$ can be expressed in terms of the quantities associated with the symmetric nuclear matter as follows [3,16,39]:

$$t_0 = \frac{8}{\rho_{\rm nm}}\left\{\frac{\left[-B/A + (2m/m^*-3)(\hbar^2/10m)k_f^2\right]\left[\frac{1}{27}K_{\rm nm} - (1-6m^*/5m)(\hbar^2/9m^*)k_f^2\right]}{-B/A + \frac{1}{9}K_{\rm nm} - (4m/3m^*-1)(\hbar^2/10m)k_f^2} + \left(1-\frac{5m}{3m^*}\right)\frac{\hbar^2}{10m}k_f^2\right\}, \tag{27}$$

$$t_1 = \frac{2}{3}[T_0 + T_s], \tag{28}$$

$$t_2 = t_1 + \frac{8}{3}\left[\left(\frac{1}{4}t_0 + \frac{1}{24}t_3\rho_{\rm nm}^{\alpha}\right)\frac{2m^*}{\hbar^2}\frac{k_f}{\pi^2} + G_0'\right]\frac{\hbar^2}{m^*\rho_{\rm nm}}, \tag{29}$$

$$t_3 = \frac{16}{\rho_{\rm nm}^{\alpha+1}}\frac{\left[-B/A + (2m/m^* - 3)(\hbar^2/10m)k_f^2\right]^2}{-B/A + \frac{1}{9}K_{\rm nm} - (4m/3m^* - 1)(\hbar^2/10m)k_f^2}, \tag{30}$$

$$x_0 = \frac{4}{t_0\rho_{\rm nm}}\left\{\frac{\hbar^2}{6m}k_f^2 - \frac{1}{24}t_3\left(x_3 + \frac{1}{2}\right)\rho_{\rm nm}^{\alpha+1} + \frac{1}{24}[t_2(4 + 5x_2) - 3t_1x_1]\rho_{\rm nm}k_f^2 - J\right\} - \frac{1}{2}, \tag{31}$$

$$x_1 = \frac{1}{t_1}\left[4\frac{\hbar^2\kappa}{m\rho_{\rm nm}} - t_2(2 + x_2)\right] - 2, \tag{32}$$

$$x_2 = \frac{1}{4t_2}[8T_0 - 3t_1 - 5t_2], \tag{33}$$

$$x_3 = -\frac{8}{\alpha t_3\rho_{\rm nm}^{\alpha+1}}\left\{\frac{\hbar^2}{6m}k_f^2 - \frac{1}{12}[(4 + 5x_2)t_2 - 3t_1x_1]\rho_{\rm nm}k_f^2 - 3J + L\right\} - \frac{1}{2}, \tag{34}$$

$$\alpha = \frac{B/A - \frac{1}{9}K_{\rm nm} + (4m/3m^* - 1)(\hbar^2/10m)k_f^2}{-B/A + (2m/m^* - 3)(\hbar^2/10m)k_f^2}, \tag{35}$$

where

$$T_0 = \frac{1}{8}[3t_1 + (5 + 4x_2)t_2] = \frac{\hbar^2}{m\rho_{\rm nm}}\left(\frac{m}{m^*} - 1\right), \tag{36}$$

$$T_s = \frac{1}{8}[9t_1 - (5 + 4x_2)t_2], \tag{37}$$

and

$$k_f = \left(\frac{3\pi^2}{2}\rho_{\rm nm}\right)^{1/3}. \tag{38}$$

In Eqs. (27)–(35), the various quantities characterizing the nuclear matter are the binding energy per nucleon $B/A$, isoscalar effective mass $m^*/m$, nuclear matter incompressibility coefficient $K_{\rm nm}$, symmetry-energy coefficient $J = S(\rho = \rho_{\rm nm})$, the coefficient $L = P(\rho = \rho_{\rm nm})$, enhancement factor $\kappa$, and Landau parameter $G_0'$. All these quantities are taken at the saturation density $\rho_{\rm nm}$. It must be pointed out that the expression for the parameter $G_0'$ used in Eq. (29) includes the contributions from the spin-density term present in the Skyrme energy-density functional [22]. Therefore, for consistency, the HF calculations are also performed with the contributions from the spin density included. Once $T_0$ is known, $T_s$ can be calculated for a given value of the surface energy $E_s$ as [16]

$$E_s = 8\pi r_0^2\int_0^{\rho_{\rm nm}} d\rho\left[\frac{\hbar^2}{36m} - \frac{5}{36}T_0\rho + \frac{1}{8}T_s\rho - \frac{m^*}{\hbar^2}V_{\rm so}\rho^2\right]^{1/2} \times [B(\rho_{\rm nm})/A - B(\rho)/A]^{1/2}, \tag{39}$$

where $B(\rho)/A$ is the binding energy per nucleon given by

$$\frac{B(\rho)}{A} = -\left[\frac{3\hbar^2}{10m^*}k_f^2 + \frac{3}{8}t_0\rho + \frac{1}{16}t_3\rho^{\alpha+1}\right] \tag{40}$$

and,

$$r_0 = \left[\frac{3}{4\pi\rho_{\rm nm}}\right]^{1/3}, \tag{41}$$

$$V_{\rm so} = \frac{9}{16}{W_0}^2. \tag{42}$$

The manner in which Eqs. (27)–(35) can be used to evaluate the Skyrme parameters $t_i, x_i$, and $\alpha$ is as follows. At first, the parameters $t_0$ and $\alpha$ can be calculated in terms of $B/A$, $\rho_{\rm nm}$, $K_{\rm nm}$ and $m^*/m$ by use of Eqs. (27) and (35). Then the parameter $t_3$ can be determined with Eq. (30). Next, $T_0$ and $T_s$ can be calculated with Eqs. (36) and (39), respectively. Once the combinations $T_0$ and $T_s$ of the Skyrme parameters are known, one can calculate the remaining parameters in the following sequence: $t_1, t_2, x_2, x_1, x_3$, and $x_0$.

## IV. SIMULATED-ANNEALING-BASED ALGORITHM FOR THE MINIMIZATION OF $\chi^2$

The SAM is a generalization of a Monte Carlo technique, based on the Metropolis algorithm [40], initially developed for examining the EOS of a many-body system. The concept of SAM is based on the manner in which liquids freeze or metals recrystallize in the process of annealing. In an annealing process, a metal, initially at high temperature and disordered, slowly cools so that the system at any time is in thermodynamic equilibrium. As cooling proceeds, the system becomes more ordered and approaches a frozen ground state at zero temperature.

With this brief background, we now implement the SAM to search for the global minimum of the $\chi^2$ function as given by Eq. (2). One of the crucial key ingredients required for implementing the SAM, in the present case, is to specify the lower and the upper limits for each of the Skyrme parameters, so that the global minimum for the $\chi^2$ is searched within these limits. However, from the literature (e.g., see Refs. [8,39]) we find that the Skyrme parameters vary over a wide range. To make the search process more efficient, we make use of the fact that most of the Skyrme parameters can be expressed in terms of the various quantities related to the nuclear matter properties as described in Sec. III. Most of these nuclear matter quantities are known empirically within 10–20%. For convenience , we define a vector $\mathbf{v}$ with the components as

$$\mathbf{v} \equiv (B/A, K_{\rm nm}, \rho_{\rm nm}, m^*/m, E_s, J, L, \kappa, G_0', W_0). \tag{43}$$

Once the vector $\mathbf{v}$ is known we can calculate the values of all the Skyrme parameters as discussed in Sec. III. We also define the vectors $\mathbf{v}_0$, $\mathbf{v}_1$, and $\mathbf{d}$. The vectors $\mathbf{v}_0$ and $\mathbf{v}_1$ contain the lower and the upper limits of each of the components of the vector $\mathbf{v}$. The vector $\mathbf{d}$ represents the maximum displacement allowed in a single step for the components of the vector $\mathbf{v}$. We implement the SAM algorithm by using the following basic steps,

(i) We start with a guess value for the vector **v** and calculate $\chi^2$ (say, $\chi^2_{\rm old}$) using Eq. (2) for a given set of the experimental data and the corresponding HF results together with the theoretical errors.

(ii) We generate randomly a new set of Skyrme parameters by using the following steps. First, we use a uniform random number to select a component $v_r$ of the vector **v**. Second, the randomly selected component $v_r$ is then assigned a new value,

$$v_r \rightarrow v_r + \eta d_r, \tag{44}$$

where $\eta$ is a uniform random number that lies within the range of $-1$ to $+1$. The second step is repeated until the new value of $v_r$ is found within its allowed limits defined by $\mathbf{v}_0$ and $\mathbf{v}_1$. We use this modified **v** to generate a new set of Skyrme parameters. It may be noted that a change in the value of a component of the vector **v** may lead to changes in the values of several Skyrme parameters. For example, a change in the value of $K_{\rm nm}$ will alter the values of the Skyrme parameters $t_0$, $t_3$ and $\alpha$.

(iii) The newly generated set of the Skyrme parameters is accepted by use of the Metropolis algorithm as follows. We calculate the quantity

$$\mathcal{P}(\chi^2) = e^{(\chi^2_{\rm old}-\chi^2_{\rm new})/T}, \tag{45}$$

where we obtain $\chi^2_{\rm new}$ by using the newly generated set of the Skyrme parameters and $T$ is a control parameter (an effective temperature). The new set of Skyrme parameters is accepted only if

$$\mathcal{P}(\chi^2) > \beta, \tag{46}$$

where $\beta$ is a uniform random number that lies between 0 and 1. If the new Skyrme parameters are accepted [i.e., condition (46) is satisfied], it is called a "successful reconfiguration."

To search for the global minimum of $\chi^2$ we begin with some reasonable value of an effective temperature $T = T_i$. For a given $T_i$, we repeat steps (ii) and (iii) for, say, $100N_p$ reconfigurations, or for $10N_p$ successful reconfigurations, whichever comes first. Then we reduce the temperature by following a suitable annealing schedules. One encounters various annealing schedules available in the literature such as linear, exponential, Boltzmann, and Cauchy [13]. Among these, the Boltzmann annealing schedule is the slowest one and the exponential annealing schedule is the fastest one. In the present work we have employed the Cauchy annealing schedule given by

$$T(k) = T_i/ck, \tag{47}$$

where $c$ is a constant, which is taken to be unity in the present work, and $k = 1, 2, 3, \ldots$, is the time index. We keep on reducing the value of $T$ by using Eq. (47) in the subsequent steps until the effort to reduce the value of $\chi^2$ further becomes sufficiently discouraging.

In Table I we list the values of all the components of the vectors **v**, $\mathbf{v}_0$, $\mathbf{v}_1$, and **d** used in the numerical computation. We have varied the components of the vector **v** over a wide range. The values of the maximum displacement as defined by the components of **d** are so chosen that the corresponding component of the vector **v** can be varied over the entire range given by the vectors $\mathbf{v_0}$ and $\mathbf{v_1}$, within the adopted number of reconfigurations. We have carried out several sample runs and found that $T_i = 1.25$ along with the Cauchy annealing schedule yields reasonable values of the Skyrme parameters. We must mention here that the range for the quantities $L, \kappa$, and $G'_0$ as given in Table I is so chosen that they vary within acceptable limits [17].

TABLE I. Values of the components of the vectors **v**, $\mathbf{v}_0$, $\mathbf{v}_1$, and **d** used for implementing the SAM-based algorithm for searching the global minimum of $\chi^2$. The vector **v** initializes the value of $\chi^2$, whereas $\mathbf{v}_0$ and $\mathbf{v}_1$ limit the search space for the Skyrme parameters. The components of the vector **d** correspond to the maximum displacements allowed for the reconfiguration.

| | **v** | $\mathbf{v}_0$ | $\mathbf{v}_1$ | **d** |
|---|---|---|---|---|
| $B/A$ (MeV) | 16.0 | 17.0 | 15.0 | 0.40 |
| $K_{\rm nm}$ (MeV) | 230.0 | 200.0 | 300.0 | 20.0 |
| $\rho_{\rm nm}$ (fm$^{-3}$) | 0.160 | 0.150 | 0.170 | 0.005 |
| $m^*/m$ | 0.70 | 0.60 | 0.90 | 0.04 |
| $E_s$ (MeV) | 18.0 | 17.0 | 19.0 | 0.3 |
| $J$(MeV) | 32.0 | 25.0 | 40.0 | 4.0 |
| $L$ (MeV) | 47.0 | 20.0 | 80.0 | 10.0 |
| $\kappa$ | 0.25 | 0.1 | 0.5 | 0.1 |
| $G'_0$ | 0.08 | 0.00 | 0.40 | 0.10 |
| $W_0$ (MeV fm$^5$) | 120.0 | 100.0 | 150.0 | 5.0 |

## V. EXPERIMENTAL DATA AND SOME CONSTRAINTS

In this section we discuss our selection of the experimental data and the corresponding theoretical errors adopted in the $\chi^2$ fit, Eq. (2), to the HF results. In Table II we summarize our choice of the experimental data. It must be noted that, in addition to the typically used data on the binding energy, charge radii, and spin-orbit splitting, we also include in our fit the experimental data for the radii of valence neutron orbits and the breathing-mode energies of several nuclei. All of these experimental data are taken from Refs. [41–47]. For the binding energy we use in our fit the error of 1.0 MeV, except for the $^{100}$Sn nuclei. The binding energy for the $^{100}$Sn nucleus is determined from systematics and is expected to have large errors. Thus we assign it a theoretical error of 2.0 MeV. For the charge rms radii we use the theoretical error of 0.02 fm except for the case of $^{56}$Ni nucleus. The charge rms radii for the $^{56}$Ni nucleus is obtained from systematics and we use the theoretical error of 0.04 fm. We consider in our fit the experimental data for the spin-orbit splittings for the $2p$ neutrons and protons in the $^{56}$Ni nucleus and the rms radii for the $1d_{5/2}$ and $1f_{7/2}$ neutron orbits in $^{17}$O and $^{41}$Ca nuclei, respectively. We use [46]

$$\epsilon(2p_{1/2}) - \epsilon(2p_{3/2}) = \begin{cases} 1.88 \text{ MeV, neutrons} \\ 1.83 \text{ MeV, Protons} \end{cases}, \tag{48}$$

where $\epsilon$ is the "bare" single-particle energy we obtain by unfolding the experimental data for the energy levels in $^{57}$Ni and $^{57}$Cu nuclei by appropriately accounting for the coupling

TABLE II. Selected experimental data for the binding energy $B$, charge rms radius $r_{\rm ch}$, rms radii of valence neutron orbits $r_v$, spin-orbit splitting S-O, breathing-mode constrained energy $E_0$, and critical density $\rho_{\rm cr}$ used in the fit to determine the parameters of the Skyrme interaction.

| Properties | Nuclei | Ref. |
|---|---|---|
| $B$ | $^{16,24}$O, $^{34}$Si, $^{40,48}$Ca, $^{48,56,68,78}$Ni, $^{88}$Sr, $^{90}$Zr, $^{100,132}$Sn, $^{208}$Pb | [41] |
| $r_{\rm ch}$ | $^{16}$O, $^{40,48}$Ca, $^{56}$Ni, $^{88}$Sr, $^{90}$Zr, $^{208}$Pb | [42,43] |
| $r_v(\nu 1d_{5/2})$ | $^{17}$O | [44] |
| $r_v(\nu 1f_{7/2})$ | $^{41}$Ca | [45] |
| S-O | $2p$ orbits in $^{56}$Ni | [46] |
| $E_0$ | $^{90}$Zr, $^{116}$Sn, $^{144}$Sm, $^{208}$Pb | [47] |
| $\rho_{\rm cr}$ | Nuclear matter | See text |

to core excitations. Of course, it is more appropriate to use the splitting of high $l$ orbits in a heavy nucleus (e.g., $^{208}$Pb nucleus) to determine the strength of the spin-orbit interaction. However, to the best of our knowledge, unlike for the $^{56}$Ni nucleus, the bare single-particle energies for the heavier nuclei are not available. For the rms radii of the valence neutron orbits in $^{17}$O and $^{41}$Ca nuclei we use $r_v(\nu 1d_{5/2}) = 3.36$ fm and $r_v(\nu 1f_{7/2}) = 3.99$ fm, [44,45] respectively. The theoretical error taken for the spin-orbit splitting data is 0.2 MeV, and for the rms radii for the valence neutron orbits we use the experimental error of 0.06 fm. We must point out that the choice of the theoretical error on the rms radii for the valence neutron orbits is due to the large uncertainties associated with their extraction from the experimental measurements. To be consistent with the way these valence neutron radii are determined, we do not include the c.m. correction to these data. The experimental data for the breathing-mode constrained energies $E_0$ included in our fit are 17.81, 15.90, 15.25, and 14.18 MeV for the $^{90}$Zr, $^{116}$Sn, $^{144}$Sm, and $^{208}$Pb nuclei [47], respectively, with the theoretical error taken to be 0.5 MeV for the $^{90}$Zr nucleus and 0.3 MeV for the other nuclei. We also include the critical density $\rho_{\rm cr}$ in the fit, assuming a value of $2.5\rho_0$ with an error of $0.5\rho_0$. Further the values of the Skyrme parameters are constrained by the requirement that (i) $P \geqslant 0$ for $\rho \leqslant 3\rho_0$, (ii) $\kappa = 0.1 - 0.5$, and (iii) $G_0' \geqslant 0$ at $\rho = \rho_0$.

## VI. RESULTS AND DISCUSSIONS

In the preceding sections we have described in detail the implementation of the SAM-based algorithm to fit the values of the Skyrme parameters to a given set of the experimental data considered in this work. We have carried out two different fits. These fits are carried out with the same set of experimental data along with some constraints as discussed in Sec. V. We name these fits (i) KDE0, in which only the Coulomb direct term in the form of Eq. (13) is included; and (ii) KDE, in which the direct as well as the Coulomb exchange terms are included [Eqs. (12)–(14)].

The c.m. corrections to the total binding energy, Eqs. (16) and (17), and the charge rms radii, Eqs. (18) and (19), are carried out with the schemes described in Sec. II B.

We first consider some technical aspects required for implementing the SAM. As is evident from Sec. IV, there are two crucial ingredients, namely (i) initial value for the control parameter $T = T_i$ and (ii) an annealing schedule that determines the subsequent value for $T$. These ingredients essentially control the computer time and the quality of the final fit. If one starts with a smaller value for $T_i$ and/or uses a faster annealing schedule, one may not be able to hit the global minimum of the objective function and rather get trapped in one of the local minima. In the present work we have employed the Cauchy annealing schedule. We have carried out several trial calculations and find that $T_i = 1.25$, along with the Cauchy annealing schedule as given by expression (47), yields reasonable values for the best-fit parameters. To validate the present approach we carried out the following checks. Starting with the final values of the Skyrme parameters we obtained by using the SAM, we attempted to minimize further the value of $\chi^2$ by using the Levenberg-Marquardt (LM) method [10] as conventionally used. However, we found no further decrease in the value of the $\chi^2$. As an illustration, we plot in Fig. 1 the average value $\langle \chi^2 \rangle_T$ as an inverse function of the control parameter $T$ for the KDE0 case. The curves labeled $v$ and $v_1$ represent the results obtained from two different choices of the

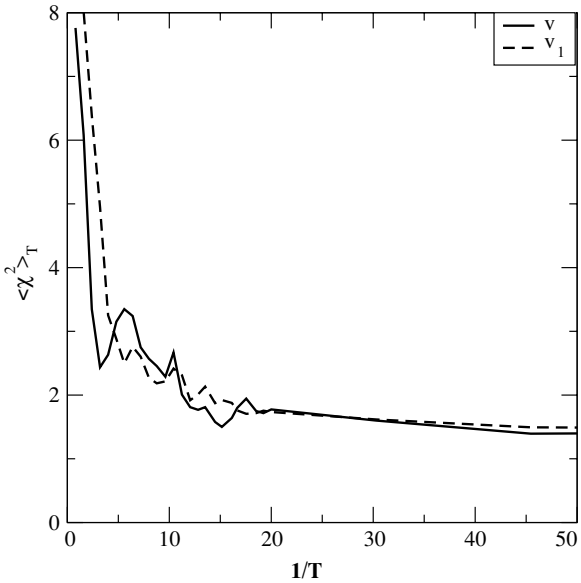


FIG. 1. Variation of the average value of $\langle \chi^2 \rangle_T$ as a function of the inverse of the control parameter $T$ for the KDE0 interaction for the two different choices of the starting parameters (see text for details).

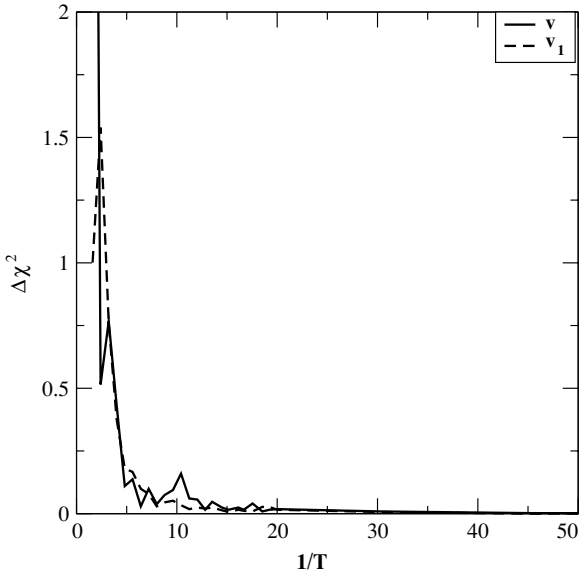


FIG. 2. Variation of the fluctuations $\Delta\chi_T^2$ in the value of $\chi^2$ as a function of $1/T$ for the KDE0 interaction for the two different choices of the starting parameters (see text for details).

starting values for the Skyrme parameters. The initial value of the Skyrme parameters for the curve labeled $v$ (solid curve) and $v_1$ (dashed curve) are obtained with the set of values given in the second and fourth columns of Table I, respectively. The value of $\langle\chi^2\rangle_T$ is obtained by averaging over all the successful reconfigurations for a given $T$. We see from Fig. 1 that the value of $\langle\chi^2\rangle_T$ shows a remarkable decrease at initial stages and then oscillates before saturating to a minimum value for $T \leqslant 0.05$. The value of $\chi^2$ at lower $T$ is more or less independent of the starting values for the Skyrme parameters. In Fig 2 we show the variation of $\Delta\chi_T^2 = \langle(\chi^2 - \langle\chi^2\rangle)^2\rangle_T$ as an inverse function of $T$. We see that the fluctuations in the value of $\chi^2$ is large for larger values of $T$. As $T$ decreases, fluctuations in the value of $\chi^2$ also decrease rapidly. This means that initial value for $T$ should not be too small, because at smaller $T$ it is less likely to jump from a configuration with lower value of $\chi^2$ to one having a higher value. As a result, one may get trapped in a local minima. In Table III we give the values of the parameters for the KDE0 interaction at the minimum value of the $\chi^2$ obtained from different choices for the starting values for the Skyrme parameters. It is interesting to note that not only is the final value of the $\chi^2$ less sensitive to the choice of the initial parameters, but the resulting Skyrme parameters are also quite close. In what follows, we present the results for the KDE0 and KDE interactions. The starting (or guess) values for the Skyrme parameters used to generate these interactions are obtained from the nuclear matter quantities given in the second column of the Table I.

In Table IV we give the values for the various quantities characterizing the nuclear matter obtained at the minimum value of the $\chi^2$. We also note that the values of all the nuclear matter properties for the KDE0 and KDE Skyrme interactions are closer to those obtained for the SLy7 interaction. However, it is worth mentioning that the values of the $K_{\rm nm}$ and $m^*/m$ for both the interactions generated here emerge from the fit,

TABLE III. Comparison of the parameters for the KDE0 interaction at the minimum value of $\chi^2$ obtained from different choices for the starting values of the Skyrme parameters.

| Parameter | KDE0(**v**) | KDE0($\mathbf{v}_1$) |
|---|---|---|
| $t_0$ (MeV·fm$^3$) | −2526.5110 | −2553.0843 |
| $t_1$ (MeV·fm$^5$) | 430.9418 | 411.6963 |
| $t_2$ (MeV·fm$^5$) | −398.3775 | −419.8712 |
| $t_3$ (MeV·fm$^{3(1+\alpha)}$) | 14235.5193 | 14603.6069 |
| $x_0$ | 0.7583 | 0.6483 |
| $x_1$ | −0.3087 | −0.3472 |
| $x_2$ | −0.9495 | −0.9268 |
| $x_3$ | 1.1445 | 0.9475 |
| $W_0$ (MeV·fm$^5$) | 128.9649 | 124.4100 |
| $\alpha$ | 0.1676 | 0.1673 |

unlike the SLy type interactions for which the values for these quantities were kept fixed. In our fits, the values of $K_{\rm nm}$ and $m^*/m$ are mainly constrained by the inclusion of the experimental data on breathing-mode energy and the value of critical density $\rho_{\rm cr} = 2.5\rho_0 \pm 0.5\rho_0$ [16,17]. In the last row of this table we give the values of $\chi^2$ at the minimum. For the sake of completeness, we list in Table V the values of the Skyrme parameters obtained in the fits. One can easily calculate the values of these Skyrme parameters by using the various nuclear matter quantities given in Table IV, as described in Sec. III. In Table V we also give in parentheses the values of the standard deviations for the Skyrme parameters. Because, within the SAM algorithm one cannot calculate these standard deviations in a straightforward manner, we resort to some alternative approach. We have determined the values of the standard deviations on the parameters for the KDE0 and KDE interactions by using the LM method. The LM method requires two inputs, namely, a set of the experimental data and the starting values of the interaction parameters. The set of experimental data is taken to be exactly the same as the one used to generate the KDE0 and KDE interactions. The starting values of the interactions parameters used are the ones obtained by use of SAM for the KDE0 and KDE interactions.

In Table VI we present our results for the deviation $\Delta B = B^{\rm exp} - B^{\rm th}$ for the values of the binding energy obtained from the newly generated KDE0 and KDE interactions. Similar

TABLE IV. Nuclear matter properties for the KDE0 and KDE interactions at $\chi^2 = \chi^2_{\rm min}$.

| Parameter | KDE0 | KDE | SLy7 |
|---|---|---|---|
| $B/A$ (MeV) | 16.11 | 15.99 | 15.92 |
| $K_{\rm nm}$ (MeV) | 228.82 | 223.89 | 229.7 |
| $\rho_{\rm nm}$ | 0.161 | 0.164 | 0.158 |
| $m^*/m$ | 0.72 | 0.76 | 0.69 |
| $E_s$ (MeV) | 17.91 | 17.98 | 17.89 |
| $J$ (MeV) | 33.00 | 31.97 | 31.99 |
| $L$ (MeV) | 45.22 | 41.43 | 47.21 |
| $\kappa$ | 0.30 | 0.16 | 0.25 |
| $G'_0$ | 0.05 | 0.03 | 0.04 |
| $\chi^2_{\rm min}$ | 1.3 | 2.2 | |

TABLE V. The values of the Skyrme parameters for KDE0 and KDE interactions obtained by minimization of the $\chi^2$. For the sake of comparison we have also listed the values of the parameters for the SLy7 interaction. The values in parentheses are the standard deviations for the corresponding Skyrme parameters.

| Parameter | KDE0 | KDE | SLy7 |
|---|---|---|---|
| $t_0$ (MeV·fm$^3$) | −2526.5110 (140.6256) | −2532.8842 (115.3165) | −2482.41 |
| $t_1$ (MeV·fm$^5$) | 430.9418 (16.6729) | 403.7285 (27.6336) | 457.97 |
| $t_2$ (MeV·fm$^5$) | −398.3775 (27.3099) | −394.5578 (14.2610) | −419.85 |
| $t_3$ (MeV·fm$^{3(1+\alpha)}$) | 14235.5193 (680.7344) | 14575.0234 (641.9932) | 13677.0 |
| $x_0$ | 0.7583 (0.0655) | 0.7707 (0.0579) | 0.8460 |
| $x_1$ | −0.3087 (0.0165) | −0.5229 (0.0298) | −0.5110 |
| $x_2$ | −0.9495 (0.0179) | −0.8956 (0.0270) | −1.0000 |
| $x_3$ | 1.1445 (0.0862) | 1.1716 (0.0767) | 1.3910 |
| $W_0$ (MeV·fm$^5$) | 128.9649 (3.3258) | 128.0572 (4.3943) | 126.00 |
| $\alpha$ | 0.1676 (0.0163) | 0.1690 (0.0144) | 0.1667 |

deviations $\Delta r_{\rm ch}$ for the charge rms radii are presented in Table VII. For comparison, in the last columns of these tables we give the values of $\Delta B$ and $\Delta r_{\rm ch}$ for the SLy7 interaction, taken from Ref. [4]. One can easily verify from Table VI that the magnitude of the deviations for the binding energy for most of the cases is much less than 0.5% in the case of KDE0 interaction. The KDE interaction yields larger error in the values of the binding energy (∼0.6–1.0%) for the $^{16}$O, $^{48}$Ni, and $^{100}$Sn nuclei. We would also like to remark here that, in determining the SKX interaction, the binding energy for the $^{56}$Ni nucleus was not considered in the fit and that for the $^{100}$Sn nucleus was included in the fit with a theoretical error of 1.0 MeV. We find that if one attempts to do so, the binding energy for the $^{56}$Ni becomes off by more than 3 MeV. We see from Table VII that, except for the $^{16}$O and $^{48}$Ca nuclei, the deviations in the values of the charge rms radii for the KDE0 interaction is less than 0.5%. In addition to the binding energy and the charge rms radii of the nuclei used in our fits, we have also considered a few more experimental data, as discussed in Sec. V. In Tables VIII and IX we present our results for these additional quantities. The values of $\rho_{\rm cr}$ are greater than $2\rho_0$. The values for the radii of valence neutron orbits and the spin-orbit splittings considered in our fits are quite reasonable for all the interactions considered here. It can be seen from Table IX that our fit to the breathing-mode constrained energies is overall in reasonable agreement with the corresponding experimental data.

We now consider our results for the binding-energy difference between the $^{48}$Ca and $^{48}$Ni mirror nuclei. One may verify from Table VI that the binding-energy difference $B(^{48}\text{Ca}) - B(^{48}\text{Ni}) = 67.23$ and 64.02 MeV for the KDE0 and KDE interactions, respectively, compared with the experimental value of 68.85 MeV. We would also like to add that the said difference for the SKX interaction is 66.3 MeV, which is 1.0 MeV lower than our most realistic KDE0 interaction.

TABLE VI. Results for the total binding-energy $B$ (in mega-electron-volts) for several nuclei. The experimental data $B^{\rm exp}$ used to fit the Skyrme parameters were taken from [41]. The theoretical error $\sigma$ was taken to be 2.0 MeV for the $^{100}$Sn nucleus and 1.0 MeV for the other nuclei. In the third and fourth columns we give the values for $\Delta B = B^{\rm exp} - B^{\rm th}$ obtained from our new fits. The last column contains the values for $\Delta B$ for the SLy7 Skyrme interaction taken from Ref. [4].

| Nuclei | $B^{\rm exp}$ | $\Delta B = B^{\rm exp} - B^{\rm th}$ | | |
|---|---|---|---|---|
| | | KDE0 | KDE | SLy7 |
| $^{16}$O | 127.620 | 0.394 | 1.011 | −0.93 |
| $^{24}$O | 168.384 | −0.581 | 0.370 | |
| $^{34}$Si | 283.427 | −0.656 | 0.060 | |
| $^{40}$Ca | 342.050 | 0.005 | 0.252 | −2.85 |
| $^{48}$Ca | 415.990 | 0.188 | 1.165 | 0.11 |
| $^{48}$Ni | 347.136 | −1.437 | −3.670 | |
| $^{56}$Ni | 483.991 | 1.091 | 1.016 | 1.71 |
| $^{68}$Ni | 590.408 | 0.169 | 0.539 | 1.06 |
| $^{78}$Ni | 641.940 | −0.252 | 0.763 | |
| $^{88}$Sr | 768.468 | 0.826 | 1.132 | |
| $^{90}$Zr | 783.892 | −0.127 | −0.200 | |
| $^{100}$Sn | 824.800 | −3.664 | −4.928 | −4.83 |
| $^{132}$Sn | 1102.850 | −0.422 | −0.314 | 0.08 |
| $^{208}$Pb | 1636.430 | 0.945 | −0.338 | −0.33 |

TABLE VII. Results for the charge rms radii $r_{\rm ch}$ (in femtometers). The experimental data used in the fit to determine the values of the Skyrme parameters are taken from Refs. [42,43]. The theoretical error $\sigma$ is taken to be 0.04 fm for the $^{56}$Ni nucleus and 0.02 fm for the other nuclei. In the third and fourth columns we give the values for $\Delta r_{\rm ch} = r_{\rm ch}^{\rm exp} - r_{\rm ch}^{\rm th}$ obtained from our new fits. The last column contains the values for $\Delta r_{\rm ch}$ for the SLy7 Skyrme interaction taken from Ref. [4].

| Nuclei | $r_{\rm ch}^{\rm exp}$ | $\Delta r_{\rm ch} = r_{\rm ch}^{\rm exp} - r_{\rm ch}^{\rm th}$ | | |
|---|---|---|---|---|
| | | KDE0 | KDE | SLy7 |
| $^{16}$O | 2.730 | −0.041 | −0.039 | −0.017 |
| $^{40}$Ca | 3.490 | 0.000 | 0.011 | 0.020 |
| $^{48}$Ca | 3.480 | −0.021 | −0.008 | −0.015 |
| $^{56}$Ni | 3.750 | −0.018 | 0.000 | −0.008 |
| $^{88}$Sr | 4.219 | −0.002 | 0.019 | |
| $^{90}$Zr | 4.258 | −0.008 | 0.013 | |
| $^{208}$Pb | 5.500 | 0.011 | 0.041 | 0.002 |

TABLE VIII. Critical density $\rho_{\rm cr}$, rms radii of the valence neutron orbits $r_v$, and spin-orbit splitting (S-O). The experimental values (and the theoretical error $\sigma$) used in the fit to determine the Skyrme parameters are taken as follows: For $\rho_{\rm cr}$ we assume a value of $2.5\rho_0$ ($\sigma = 0.5\rho_0$); the values of $r_v$ were taken from Refs. [44,45] ($\sigma =$ 0.06 fm); and the spin-orbit values in $^{56}$Ni were taken from Ref. [46] ($\sigma = 0.2$ MeV). In columns 3−6 we give the results obtained from our new fits.

| | Experimental | KDE0 | KDE |
|---|---|---|---|
| $\rho_{\rm cr}/\rho_0$ | 2.5 | 2.5 | 2.1 |
| $r_v(\nu 1d_{5/2})$(fm) | 3.36 | 3.42 | 3.41 |
| $r_v(\nu 1f_{7/2})$(fm) | 3.99 | 4.05 | 4.03 |
| $\epsilon_n(2p_{1/2}) - \epsilon_n(2p_{3/2})$ (MeV) | 1.88 | 1.84 | 1.81 |
| $\epsilon_p(2p_{1/2}) - \epsilon_p(2p_{3/2})$ (MeV) | 1.83 | 1.64 | 1.63 |

TABLE IX. Comparison of the breathing-mode constrained energies (in mega-electron-volts) obtained for the KDE0 and KDE interactions with the experimental data.

| Nucleus | Experimental | KDE0 | KDE |
|---|---|---|---|
| $^{90}$Zr | 17.81 | 17.98 | 17.91 |
| $^{116}$Sn | 15.90 | 16.42 | 16.36 |
| $^{144}$Sm | 15.25 | 15.53 | 15.47 |
| $^{208}$Pb | 14.18 | 13.64 | 13.60 |

TABLE X. Results for the neutron skin, $r_n - r_p$ (in femtometers), for all the nuclei considered for obtaining the KDE0 and KDE interactions.

| Nuclei | $r_n - r_p$ | |
|---|---|---|
| | KDE0 | KDE |
| $^{16}$O | −0.031 | −0.025 |
| $^{24}$O | 0.510 | 0.510 |
| $^{34}$Si | 0.189 | 0.192 |
| $^{40}$Ca | −0.051 | −0.046 |
| $^{48}$Ca | 0.158 | 0.159 |
| $^{48}$Ni | −0.282 | −0.274 |
| $^{56}$Ni | −0.056 | −0.052 |
| $^{68}$Ni | 0.175 | 0.174 |
| $^{78}$Ni | 0.287 | 0.285 |
| $^{88}$Sr | 0.095 | 0.096 |
| $^{90}$Zr | 0.064 | 0.065 |
| $^{100}$Sn | −0.081 | −0.078 |
| $^{132}$Sn | 0.220 | 0.217 |
| $^{208}$Pb | 0.160 | 0.155 |

TABLE XI. Single-particle energies (in mega-electron-volts) for $^{40}$Ca nucleus.

| Orbits | Experimental | KDE0 | KDE |
|---|---|---|---|
| | Protons | | |
| $1s_{1/2}$ | −50±11 | −39.40 | −38.21 |
| $1p_{3/2}$ | – | −26.95 | −26.42 |
| $1p_{1/2}$ | −34±6 | −22.93 | −22.34 |
| $1d_{5/2}$ | — | −14.49 | −14.51 |
| $2s_{1/2}$ | −10.9 | −9.48 | −9.66 |
| $1d_{3/2}$ | −8.3 | −7.59 | −7.53 |
| $1f_{7/2}$ | −1.4 | −2.38 | −2.76 |
| | Neutrons | | |
| $1s_{1/2}$ | – | −47.77 | −46.13 |
| $1p_{3/2}$ | – | −34.90 | −33.92 |
| $1p_{1/2}$ | – | −30.78 | −29.73 |
| $1d_{5/2}$ | – | −22.08 | −21.66 |
| $2s_{1/2}$ | −18.1 | −17.00 | −16.78 |
| $1d_{3/2}$ | −15.6 | −14.97 | −14.48 |
| $1f_{7/2}$ | −8.32 | −9.60 | −9.58 |
| $2p_{3/2}$ | −6.2 | −4.98 | −5.15 |

TABLE XII. Single-particle energies (in mega-electron-volts) for $^{208}$Pb.

| Orbits | Experimental | KDE0 | KDE |
|---|---|---|---|
| | Protons | | |
| $1g_{9/2}$ | −15.43 | −17.85 | −17.34 |
| $1g_{7/2}$ | −11.43 | −13.77 | −13.39 |
| $2d_{5/2}$ | −9.70 | −11.37 | −11.23 |
| $1h_{11/2}$ | −9.37 | −9.87 | −9.68 |
| $2d_{3/2}$ | −8.38 | −9.43 | −9.30 |
| $3s_{1/2}$ | −8.03 | −8.67 | −8.62 |
| $1h_{9/2}$ | −3.77 | −4.00 | −3.99 |
| $2f_{7/2}$ | −2.87 | −2.78 | −3.00 |
| $1i_{13/2}$ | −2.16 | −1.62 | −1.72 |
| $3p_{3/2}$ | −0.95 | 0.60 | 0.26 |
| $2f_{5/2}$ | −0.47 | −0.19 | −0.42 |
| | Neutrons | | |
| $1h_{9/2}$ | −10.85 | −12.39 | −12.24 |
| $2f_{7/2}$ | −9.72 | −11.60 | −11.64 |
| $1i_{13/2}$ | −9.01 | −9.33 | −9.20 |
| $3p_{3/2}$ | −8.27 | −8.67 | −8.77 |
| $2f_{5/2}$ | −7.95 | −8.59 | −8.64 |
| $3p_{1/2}$ | −7.38 | −7.54 | −7.65 |
| $2g_{9/2}$ | −3.94 | −2.86 | −3.06 |
| $1i_{11/2}$ | −3.15 | −1.65 | −1.69 |
| $1j_{15/2}$ | −2.53 | −0.41 | −0.43 |
| $3d_{5/2}$ | −2.36 | −0.43 | −0.64 |
| $4s_{1/2}$ | −1.91 | 0.08 | −0.08 |
| $2g_{7/2}$ | −1.45 | 0.38 | 0.20 |
| $3d_{3/2}$ | −1.42 | 0.56 | 0.40 |

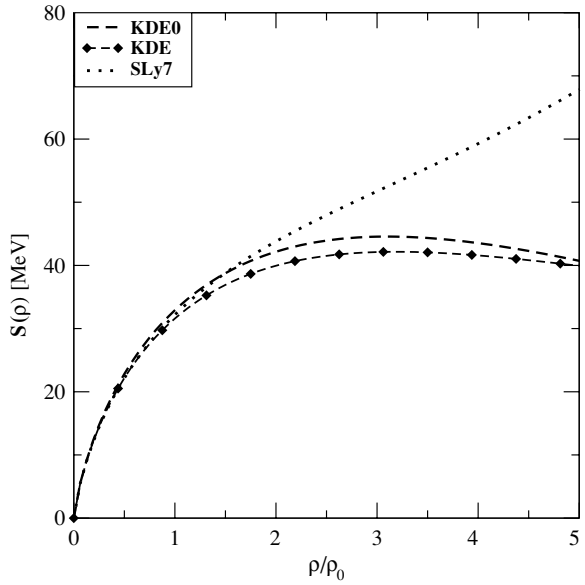


FIG. 3. Variation of the symmetry-energy coefficient $S(\rho)$ as a function of the nuclear matter density $\rho$.

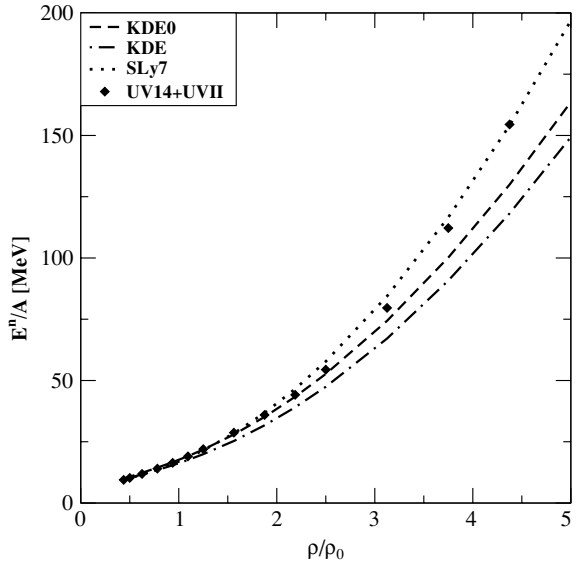


FIG. 4. Energy per particle for pure neutron matter $E^{(n)}/A$ as a function of density. Results for the two newly generated Skyrme interactions KDE0 and KDE are compared with those obtained for the SLy7 Skyrme force and the realistic UV14+UVII model of Wiringa, Fiks, and Fabrocini [53].

On the other hand, most of the Skyrme interactions that include the contribution from the exchange Coulomb term yield $B(^{48}\mathrm{Ca}) - B(^{48}\mathrm{Ni}) \approx 63$ MeV, which is 6 MeV lower than the corresponding experimental value.

We present in Table X our results for the neutron skin, $r_n - r_p$, the difference between the rms radii for the point neutrons and proton density distributions, for the KDE0 and KDE interactions. We compare in Tables XI and XII the values of the single-particle energies with the available experimental data for the $^{40}$Ca and $^{208}$Pb nuclei [48,49], respectively. We find that the single-particle energies for the occupied states near the Fermi energy compare reasonably well with the experimental ones. We would like to remark here that the HF approach alone is not expected to reproduce the experimental single-particle energie, and therefore we have not included them in our fit.

Finally, we consider the behavior of the symmetry-energy coefficient $S(\rho)$ for densities relevant to the study of neutron stars. It is well known [50,51] that the values of $S(\rho)$ and the resulting EOS for pure neutron matter at higher densities ($\rho > 2\rho_0$) are crucial in understanding the various properties of neutron star. For example, the proton fraction at any density depends strongly on the value of $S(\rho)$ at that density, which in turn affects the chemical compositions as well as the cooling mechanism of the neutron star [52]. Yet no consensus is reached for the density dependence of $S(\rho)$. We show in Fig. 3 our results for the variation of the symmetry energy $S$ as a function of the nuclear matter density $\rho$. We see that for the KDE0 and KDE interactions the value of $S$ increases with density for $\rho < 3\rho_0$. All of these interactions are quite suitable for modeling the neutron star with masses close to the canonical one [8], because they yield $S > 0$ for $\rho < 4\rho_0$. In Fig. 4 we plot the EOS for the pure neutron matter resulting from the KDE0 and KDE interactions and compare them with the ones obtained for SLy7 interaction and the realistic UV14+UVII model [53]. It is striking to note that our results for the KDE0 and KDE interactions are in harmony with the EOS for the UV14+UVII model, though, unlike in the SLy7 interaction, we did not include in our fit the neutron matter EOS of the realistic UV14+UVII interaction. This seems to be due to the constraint imposed on the quantity $P$, which is related to the slope of the symmetry-energy coefficient [see Eq. (1)].

## VII. CONCLUSIONS

We have implemented the SAM to fit the values of the parameters of the Skyrme interaction of Eq. (3) by searching for the global minimum in the hypersurface of the $\chi^2$ function, Eq. (2). To demonstrate the applicability of this method we have fitted the values of the Skyrme parameters to an extensive set of experimental data together with a few additional constraints. Our experimental data set consists of the binding energies for 14 nuclei ranging from the normal to the exotic (proton- or neutron-rich) ones, charge rms radii for 7 nuclei, spin-orbit splittings for the $2p$ proton and neutron orbits of the $^{56}$Ni nucleus, and rms radii for $1d_{5/2}$ and $1f_{7/2}$ valence neutron orbits in the $^{17}$O and $^{41}$Ca nuclei, respectively. We also include in the fit the critical density $\rho_{\mathrm{cr}}$ determined from the stability conditions for the Landau parameters. The additional constraints imposed on the Skyrme parameters are that (i) the quantity $P = 3\rho(dS/d\rho)$, directly related to the slope of the symmetry energy $S$, must be positive for densities up to $3\rho_0$, a condition imposed by the neutron star models [8]; (ii) the enhancement factor $\kappa$, associated with the TRK sum rule for the isovector giant dipole resonance, should lie in the range of $0.1-0.5$; and (iii) the Landau parameter $G_0'$, crucial for the spin properties of finite nuclei and nuclear matter, should be positive at $\rho = \rho_0$.

Using these experimental data along with the additional constrains, we have carried out two different fits named as KDE0 and KDE, as described in Sec. VI. The corrections to the binding energy and charge rms radii that were due to the c.m. motion were performed by use of simple but consistent schemes. The nuclear matter properties for both interactions proposed in the present work are obtained directly from the fit. The selection of the experimental data in conjugation with some constraints ensures that these interactions can be used to study the bulk ground-state properties of nuclei ranging from the stable to the ones near the proton and neutron drip lines, as well as the properties of neutron stars. The interactions obtained in the present work encompass the merits of the SKX and SLy types of Skyrme interactions.

Before closing, we would like to mention that the method as well as the fitting strategy presented in this work can be improved in several ways. The SAM is a very adaptive approach, and therefore it offers significant scope for further improvement. For example, in the present work we jump from one configuration to another by randomly selecting a component of the vector **v** as defined by Eq. (43). This selection was done with a uniform random number. However, one can think of performing random selection of a component of **v** by assigning more plausible weight factors to these components. One can also try out different annealing schedules to determine the rate of cooling. In the present work we employed the Cauchy annealin schedule, which yields a faster cooling rate than that of the Boltzmann schedule, but a slower rate than the exponential annealing schedule. The effects on the binding energy and radii that are due to the correlations beyond mean field [54–56] can be included in the fit. These effects are important in particular for the light nuclei. One may also include in the spin-orbit splitting the contributions that are due to the electromagnetic spin-orbit interaction [46] and modify the spin-orbit interaction by using the form proposed by Sagawa and Yoshida in Ref. [57]. Last but not least, one may also include the experimental data on the giant dipole and quadrupole resonances while fitting the Skyrme parameters in addition to the breathing-mode energy, as was done in the present work.

## ACKNOWLEDGMENTS

This work was supported in part by the U.S. Department of Energy under grant DOE-FG03-93ER40773 and the National Science Foundation under grant PHY-0355200.

[1] D. Vautherin and D. M. Brink, Phys. Rev. C **5**, 626 (1972).
[2] P. G. Reinhard and H. Flocard, Nucl. Phys. **A584**, 467 (1995).
[3] E. Chabanat, P. Bonche, P. Haensel, J. Meyer, and R. Schaeffer, Nucl. Phys. **A627**, 710 (1997).
[4] E. Chabanat, P. Bonche, P. Haensel, J. Meyer, and R. Schaeffer, Nucl. Phys. **A635**, 231 (1998).
[5] B. A. Brown, Phys. Rev. C **58**, 220 (1998).
[6] P. G. Reinhard, D. J. Dean, W. Nazarewicz, J. Dobaczewski, J. A. Maruhn, and M. R. Strayer, Phys. Rev. C **60**, 014316 (1999).
[7] M. Bender, P. H. Heenen, and P.-G. Reinhard, Rev. Mod. Phys. **75**, 121 (2003).
[8] J. R. Stone, J. C. Miller, R. Koncewicz, P. D. Stevenson, and M. R. Strayer, Phys. Rev. C **68**, 034324 (2003).
[9] S. Kirkpatrik, C. D. Gelatt, Jr., and M. P. Vecchi, Science **220**, 671 (1983).
[10] W. H. Press, S. A. Teukolsky, W. T. Vetterling, and B. P. Flannery, *Numerical Recipes in Fortran* (Cambridge University Press, New York, 1992).
[11] S. Kirkpatrik, J. Stat. Phys. **34**, 975 (1984).
[12] L. Ingber, Math. Comput. Model. **12**, 967 (1989).
[13] B. Cohen, Master's thesis, Tel-Aviv University, 1994.
[14] T. Burvenich, D. G. Madland, J. A. Maruhn, and P.-G. Reinhard, Phys. Rev. C **65**, 044308 (2002).
[15] T. J. Burvenich, D. G. Madland, and P.-G. Reinhard, Nucl. Phys. **A744**, 92 (2004).
[16] J. Margueron, J. Navarro, and N. V. Giai, Phys. Rev. C **66**, 014303 (2002).
[17] B. K. Agrawal, S. Shlomo, and V. K. Au, Phys. Rev. C **70**, 057302 (2004).
[18] B. L. Berman and S. C. Fultz, Rev. Mod. Phys. **47**, 713 (1975).
[19] H. Krivine, J. Treiner, and O. Bohigas, Nucl. Phys. **A336**, 155 (1980).
[20] K.-F. Liu, H. Luo, Z. Ma, Q. Shen, and S. A. Mozkowski, Nucl. Phys. **A534**, 25 (1991).
[21] K.-F. Liu, H. Luo, Z. Ma, and Q. Shen, Nucl. Phys. **A534**, 1 (1991).
[22] M. Bender, J. Dobaczewski, J. Engel, and W. Nazarewicz, Phys. Rev. C **65**, 054322 (2002).
[23] M. J. Giannoni and P. Quentin, Phys. Rev. C **21**, 2076 (1980).
[24] S. Shlomo, Rep. Prog. Phys. **41**, 957 (1978).
[25] S. Shlomo and W. G. Love, Phys. Scr. **26**, 280 (1982).
[26] J. A. Nolen and J. P. Schiffer, Annu. Rev. Nucl. Sci. **19**, 471 (1969).
[27] B. K. Agrawal, T. Sil, S. K. Samaddar, J. N. De, and S. Shlomo, Phys. Rev. C **64**, 024305 (2001).
[28] B. A. Brown, W. A. Richter, and R. Lindsay, Phys. Lett. **B483**, 49 (2000).
[29] M. Bender, K. Rutz, P. G. Reinhard, and J. A. Maruhn, Eur. Phys. J. A **7**, 467 (2000).
[30] G. A. Lalazissis, J. Konig, and P. Ring, Phys. Rev. C **55**, 540 (1997).
[31] P. Ring, Y. K. Gambhir, and G. A. Lalazissis, Comput. Phys. Commun. **105**, 77 (1997).
[32] W. Bertozzi, J. Friar, J. Heisenberg, and J. W. Negele, Phys. Lett. **B4**, 408 (1972).
[33] I. Sick, Phys. Lett. **B576**, 62 (2003).
[34] A. B. Migdal, *Theory of Finite Fermi Systems, and Application to Atomic Nuclei* (Interscience Pub., New York, 1967).
[35] S. Krewald, V. Klemt, J. Speth, and A. Faessler, Nucl. Phys. **A281**, 166 (1977).
[36] O. Bohigas, A. M. Lane, and J. Martorell, Phys. Rep. **51**, 267 (1979).
[37] G. Colo and N. V. Giai, Nucl. Phys. **A731**, 15c (2004).
[38] B. K. Agrawal and S. Shlomo, Phys. Rev. C **70**, 014308 (2004).

[39] J. M. G. Gomez, C. Prieto, and J. Navarro, Nucl. Phys. **A549**, 125 (1992).
[40] N. Metropolis, A. W. Rosenbluth, M. N. Rosenbluth, A. H. Teller, and E. Teller, J. Chem. Phys. **21**, 1087 (1953).
[41] G. Audi, A. H. Wapstra, and C. Thibault, Nucl. Phys. **A729**, 337 (2003).
[42] E. W. Otten, *in Treatise on Heavy-Ion Science*, edited by D. A. Bromley (Plenum, New York 1989), Vol 8.
[43] H. D. Vries, C. W. D. Jager, and C. D. Vries, At. Data Nucl. Data Tables **36**, 495 (1987).
[44] N. Kalantar-Nayestanaki, H. Baghaei, W. Bertozzi, S. Dixit, J. M. Finn, C. E. Hyde-Wright, S. Kowalski, R. W. Lourie, C. P. Sargent, P. E. Ulmer, L. Weinstein, M. V. Hynes, B. L. Berman, and J. J. Kelly, Phys. Rev. Lett. **60**, 1707 (1988).
[45] S. Platchkov, A. Amroun, P. Bricault, J. M. Cavedon, P. K. A. de Witt Huberts, P. Dreux, B. Frois, C. D. Goodman, D. Goutte, J. Martino, V. Meot, G. A. Peterson, X. H. Phan, S. Raman, and I. Sick, Phys. Rev. Lett. **61**, 1465 (1988).
[46] L. Trache, A. Kolomiets, S. Shlomo, K. Heyde, H. Dejbakhsh, C. A. Gagliardi, R. E. Tribble, X. G. Zhou, V. E. Iacob, and A. M. Oros, Phys. Rev. C **54**, 2361 (1996).
[47] D. H. Youngblood, H. L. Clark, and Y. W. Lui, Phys. Rev. Lett. **82**, 691 (1999).
[48] A. Bohr and B. R. Mottelson, *Nuclear Structure* (Benjamin, New York, 1969), Vol I.
[49] A. N. James, P. T. Andrews, P. Kirkby, and B. G. Lowe, Nucl. Phys. **A138**, 145 (1969).
[50] M. Kutschera, Phys. Lett. **B340**, 1 (1994).
[51] M. Kutschera and J. Niemiec, Phys. Rev. C **62**, 025802 (2000).
[52] J. M. Lattimer, C. J. Pethick, M. Prakash, and P. Haensel, Phys. Rev. Lett. **66**, 2701 (1991).
[53] R. B. Wiringa, V. Fiks, and A. Fabrocini, Phys. Rev. C **38**, 1010 (1988).
[54] H. Esbensen and G. F. Bertsch, Phys. Rev. C **28**, 355 (1983).
[55] S. Shlomo, Phys. Lett. **B209**, 23 (1988).
[56] M. Bender, G. F. Bertsch, and P.-H. Heenen, Phys. Rev. C **69**, 034340 (2004).
[57] H. Sagawa and S. Yoshida, Nucl. Phys. **A688**, 755 (2001).